Field-induced spin–flop transitions of interacting nanosized α-Fe_2O_3 particles dispersed in a silica glass matrix

2008 J. Phys.: Condens. Matter 20 055204

(http://iopscience.iop.org/0953-8984/20/5/055204)

J. Phys.: Condens. Matter **20** (2008) 055204 (12pp) doi:10.1088/0953-8984/20/05/055204

Field-induced spin–flop transitions of interacting nanosized α-Fe_2O_3 particles dispersed in a silica glass matrix

Sudip Mukherjee[1], Arun Kumar Pal[1], S Bhattacharya[2,3] and S Chattopadhyay[4]

[1] Department of Solid State Physics, Indian Association for the Cultivation of Science, Jadavpur, Kolkata-700 032, India
[2] Wihuri Physical Laboratory, Department of Physics, University of Turku, Finland
[3] Department of Physics, Åbo Akademi University, Turku-20500, Finland
[4] Department of Physics, Taki Government College, Taki-743429, India

E-mail: sspsm3@mahendra.iacs.res.in

Received 20 April 2007, in final form 10 December 2007
Published 14 January 2008
Online at stacks.iop.org/JPhysCM/20/055204

Abstract

Nanoparticles of 10 mol% Fe_2O_3 doped in silica glass (Fe10) samples prepared by a sol–gel method followed by calcination at various temperatures in the range 700–1000 °C are studied by x-ray, transmission electron microscopy and magnetic methods, including electron paramagnetic resonance (EPR). X-ray studies reveal the presence of both γ-Fe_2O_3 and α-Fe_2O_3 nanocrystals in varying proportion, the latter being more abundant in samples subject to calcination at higher temperature. Nanocrystals have mean sizes in the range 10–40 nm and are larger in the samples calcined at higher temperatures. The relatively narrow EPR line having its origin in superparamagnetism is observed at room temperature and is transformed to an asymmetrically broad ferromagnetic resonance signal at 77 K. Mössbauer spectra of the 700 °C calcined sample at room temperature show two doublet structures due to γ-Fe_2O_3 and α-Fe_2O_3 nanoparticles signifying their superparamagnetic character, whereas those of samples calcined at higher temperatures ($\leqslant$1000 °C) display two sextets indicating that the nanoparticles are magnetically ordered. At higher calcination temperatures ($\geqslant$900 °C) the hyperfine lines become asymmetrically broadened and the average hyperfine field diminishes in a way typical for interacting magnetic nanoparticles. Zero-field-cooled magnetization and hysteresis studies of Fe10 samples calcined at higher temperatures ($\geqslant$800 °C) in the temperature range 5–300 K reveal unusual ferromagnetic behaviour with substantial magnetization and large coercivities at low temperature (5 K). The presence of a high irreversibility field and shifted hysteresis loop in the Fe10 sample calcined at 1000 °C at 5 K has been verified from field-cooled magnetization versus the magnetic field curve. Only α-Fe_2O_3 nanoparticles generated in the Fe_2O_3:SiO_2 sample calcined at 1000 °C exhibit a Morin transition like bulk α-Fe_2O_3 crystals but at a much lower temperature $\sim$100 K. Spin–flop like transitions have been observed for the first time at temperatures above the Morin temperature, possibly induced by an external dc magnetic field of appropriate magnitude in conjunction with inter-nanoparticle exchange.

(Some figures in this article are in colour only in the electronic version)

1. Introduction

In recent times magnetic nanoparticles (NPs) have been the subject of intense scientific and technological research [1, 2]. Iron oxide NPs have been extensively studied by a number of experimental techniques such as magnetic measurements [3–18], Mössbauer spectroscopy [5–11, 16, 18–25], electron paramagnetic resonance (EPR) [14, 26–29] and neutron diffraction [30]. It is revealed that the magnetic properties of NPs are extremely sensitive to interparticle interactions.

Of six known crystalline phases of iron oxides, γ-Fe_2O_3 (maghemite) and α-Fe_2O_3 (haematite) have been most extensively studied. Magnetic properties of synthesized γ-Fe_2O_3 NPs by a sol–gel method with 16.9 and 28.5 wt% Fe concentrations in the amorphous silica matrix were studied [9] by static and dynamic susceptibility and hysteresis measurements and Mössbauer spectroscopy. In Fe_2O_3 NPs having mean particle sizes in the range 4–50 nm prepared [6] by the pulsed wire evaporation method, the amounts of γ-Fe_2O_3 and α-Fe_2O_3 NPs in the sample were estimated by x-ray diffraction (XRD) to be about 70% and 30%, respectively. From magnetic measurements the coercivity (53 Oe) and the saturation magnetization (14 emu g^{-1}) were determined to be about 20% of those of the bulk γ-Fe_2O_3. EPR and field-cooled (FC) magnetization studies [29] on γ-Fe_2O_3 NPs ($\sim$2.5 nm) embedded in a polyethylene matrix have revealed anomalies near 40 K (T_F) which have been related to the spin glass (SG) freezing in the NP surface layer. The broadening of the EPR line near 25 K has been ascribed to the increase of the exchange anisotropy field in the SG state.

Besides γ-Fe_2O_3 NPs, there has been growing interest in α-Fe_2O_3 NP systems. The magnetic properties of α-Fe_2O_3 have interested researchers for many years, particularly after Morin [31] reported a phase transition from a weakly ferromagnetic (WFM) to an antiferromagnetic (AFM) state on cooling below the Morin temperature ($T_M = 260$ K). A neutron diffraction study by Shull *et al* [32] showed that α-Fe_2O_3 is, in essence, an AFM below its Néel temperature $T_N \approx 960$ K, and that the WFM $\rightarrow$ AFM transition, that Morin had observed, was in fact a temperature-driven spin–flop (SF). Below T_M, the material behaves as a uniaxial AFM with spins oriented along the trigonal [111] axis (c axis), whilst above it the spins lie in the basal plane (perpendicular to [111] axis) except for a slight spin canting ($\sim$1 min of arc) out of the plane [32, 33] which give rise to small net weak ferromagnetic moment. In the AFM state SF transitions were subsequently observed by several investigators [34–36]. Recent research has shown that nanocrystalline α-Fe_2O_3, in general, has three critical temperatures: the Néel temperature (T_N), the blocking temperature (T_B) and the Morin temperature (T_M). Between T_B and T_N ($T_B < T_N$), the intraparticle atomic moments lock together cooperatively and order antiferromagnetically under the influence of exchange interaction and the system responds reversibly or superparamagnetically to changes in the applied field within the timescale of the measurement for the disordered individual NP moments. In DC magnetization (zero-field-cooled; ZFC) measurements, there is always a maximum at T_B. α-Fe_2O_3 NPs may also go through the Morin transition at a lower temperature (usually, $T_M < T_B$), above which the spins lie in one of the vertical planes of symmetry, and a weak ferromagnetism appears due to a slight angle between the spins of the two magnetic sublattices and, at temperatures below the T_M, two magnetic sublattices are oriented along the rhombohedral [111] axis and are exactly antiparallel. It is well known that T_M is sensitive to the sizes of the structural domains in α-Fe_2O_3. For example, T_M is less than 4 K for spherical/acicular α-Fe_2O_3 NPs having diameters in the range 8–20 nm [12, 20, 24, 37–39]. Strains, crystal defects (e.g. low crystallinity of the NPs, vacancies), stoichiometric deviations and surface effects have been indicated as the causes of the reduction of T_M [40].

It is evident from the above that a substantial number of magnetic data on both α- and γ-phases of Fe_2O_3 NP systems have accumulated. However, it appears that there is still some dearth of magnetic data on Fe_2O_3 NPs embedded in some diamagnetic material, particularly in a silica matrix. Under the circumstances it was thought worthwhile to undertake magnetic investigations on Fe_2O_3 NPs doped in silica glass to throw more light on the nature of magnetism of the said iron oxide NPs. With this end in view, Fe_2O_3 NPs doped in SiO_2 gel–glass with 10.0 mol% dopant concentration were prepared and subjected to calcination at various temperatures. Generation of Fe_2O_3 NPs of different sizes depending on calcination temperature took place. XRD reveals that γ-Fe_2O_3 NPs are predominant in the samples calcined at lower temperatures, while α-Fe_2O_3 NPs are more abundant in the samples calcined at higher temperatures. In the present communication, the results of a systematic study of the magnetic properties of Fe_2O_3 NPs principally by means of static FC and ZFC magnetic and EPR experiments have been reported. In addition, ZFC and FC magnetic hysteresis and Mössbauer (at room temperature) measurements are also performed to give a consolidated picture of the magnetism of iron oxide NPs.

2. Experimental details

Iron oxide doped silica gel is prepared from tetraethylorthosilicate (TEOS) and dopant iron sulfate having 10.0 mol% dopant concentration (henceforth referred to as Fe10), essentially following the method of Sakka and Kamiya [41]. The molar ratio of water and TEOS is kept at 20 while that of TEOS and catalyst HCl is 100. Dry ethanol is used as the solvent. The solution, poured into a Pyrex beaker and covered with polythene sheet, is kept in the atmosphere for 7–8 days to form stiff monolithic gel. The monolithic gel is then allowed to dry further at room temperature for 4–5 weeks. Dried gels are then transferred to a programmable electric furnace. Heat treatments of these samples are then performed in air at several pre-selected temperatures up to 1000 °C, in accordance with the following schedule [42]:

$$\mathrm{RT} \xrightarrow{3.5\ \mathrm{h}} 250\,^{\circ}\mathrm{C}\ (4\ \mathrm{h}) \xrightarrow{2.5\ \mathrm{h}} 310\,^{\circ}\mathrm{C}\ (4\ \mathrm{h}) \xrightarrow{2.5\ \mathrm{h}} 440\,^{\circ}\mathrm{C}\ (16\ \mathrm{h}) \xrightarrow{2.5\ \mathrm{h}} 500\,^{\circ}\mathrm{C}\ (4\ \mathrm{h}) \xrightarrow{2.5\ \mathrm{h}} 600\,^{\circ}\mathrm{C}\ (4\ \mathrm{h}) \xrightarrow{2.5\ \mathrm{h}} 700\,^{\circ}\mathrm{C}\ (4\ \mathrm{h}) \xrightarrow{2.5\ \mathrm{h}} 800\,^{\circ}\mathrm{C}\ (4\ \mathrm{h}) \xrightarrow{2.5\ \mathrm{h}} 900\,^{\circ}\mathrm{C}\ (4\ \mathrm{h}) \xrightarrow{2.5\ \mathrm{h}} 1000\,^{\circ}\mathrm{C}\ (4\ \mathrm{h}).$$

The gel–glasses are removed from the furnace at pre-selected temperatures and are stored inside an oven maintained at 130 °C.

EPR spectra of Fe10 samples calcined at 700, 800, 900 and 1000 °C are recorded in a Varian X-band EPR spectrometer (model E-109) with 100 kHz magnetic field modulation at room temperature (RT) and liquid nitrogen temperature (LNT). Powder XRD of Fe10 glass specimens are recorded using a Seifert diffractometer (model XRD3000) with Cu Kα radiation as the source. An ultrahigh resolution

JEOL JEM-2010 analytical transmission electron microscope (TEM) is employed to record TEM of Fe10 samples calcined at 700 and 1000 °C. Samples for TEM investigation are prepared by putting a drop of ethanolic dispersion of fine powder of Fe10 samples onto an amorphous carbon substrate supported on a copper grid. The magnetization and magnetic hysteresis measurements are performed on a Cryogenics S600 superconducting quantum interference device (rf-SQUID magnetometer) with temperatures varying from 5 to 300 K with ±1.0 K thermal stability and equipped with a superconducting magnet producing fields up to ±6 T. To carry out these measurements, the sample in the powder form is packed in a pocket made from PTFE tape and fixed to a length of copper wire. Masses of the samples are chosen in the range of 8–12 mg for obtaining a good signal-to-noise ratio. Fe10 samples calcined at 700, 800, 900 and 1000 °C are first cooled in zero magnetic field down to 5 K and then magnetizations are recorded by increasing the temperature in an applied magnetic field of 200 Oe (ZFC measurements). FC curves are recorded by cooling the samples again in presence of the same field. To obtain the field dependence of the magnetization, i.e. the hysteresis loop, Fe10 samples are cooled to a specific temperature and then the sample's magnetic moment, as a function of the magnetic field with a field stabilization time of 90 s, is recorded in the magnetic field range of ±6 T. Fe10 samples are studied at room temperature and 100 K by ^{57}Fe Mössbauer spectroscopy using a constant-acceleration spectrometer with source of ^{57}Co in rhodium. The spectra are obtained using a temperature-controlled liquid nitrogen cryostat. The spectrometer is calibrated with a 12.5 μm thick α-Fe foil at room temperature.

3. Results and discussions

3.1. XRD spectra and TEM

XRD patterns of Fe10 samples calcined at 700, 800, 900 and 1000 °C, recorded at a scanning rate of 0.02° s^{-1} in the 2θ range from 25° to 40°, have clearly exhibited most intense characteristic lines corresponding to α-Fe_2O_3 at $2\theta = 33.113°$ (104) (JCPDF no. 240 072) of unit cell parameters $a = 5.038$ Å, $c = 13.77$ Å (S.G.: $R\bar{3}$ (148)) and corresponding to γ-Fe_2O_3 at $2\theta = 35.399°$ (311) of unit cell parameters $a = 8.351$ Å (S.G.: $P4_132(213)$) (JCPDF No. 391 346) (figure 1).

XRD lines due to α-Fe_2O_3 and γ-Fe_2O_3 crystals have significant line broadening, indicating that the crystal sizes are most likely in the nanometre range. Most prominent (104) and (311) lines observed in the 2θ range 25°–40° arise respectively due to α-Fe_2O_3 and γ-Fe_2O_3 crystals. Applying the well-known Scherrer equation, sizes of Fe_2O_3 crystals are estimated from the integral breadths of the lines. It is confirmed that the sizes of α-Fe_2O_3 and γ-Fe_2O_3 crystals embedded in the silica glass matrix indeed lie in the nanometre range (10–40 nm) and are larger at higher calcination temperatures. It is observed that at higher calcined temperature the α-Fe_2O_3 line becomes more intense while the γ-Fe_2O_3 line weakens. However, the conversion of γ-Fe_2O_3 NPs to α-Fe_2O_3 NPs is not complete at the highest calcination temperature,

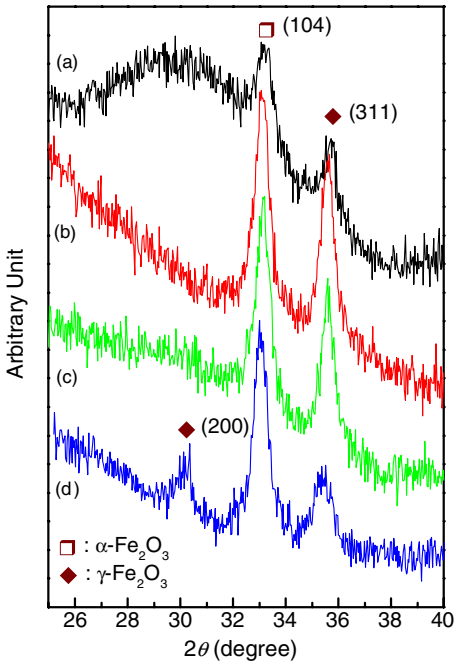

Figure 1. X-ray diffraction patterns of Fe10 samples calcined at (a) 700 °C, (b) 800 °C, (c) 900 °C and (d) 1000 °C.

i.e. 1000 °C, employed in our investigation. This is in sharp contrast with the findings in the case of bare Fe_2O_3 NPs, i.e. not embedded in any diamagnetic matrix like silica [43]. Here γ-Fe_2O_3 NPs transform irreversibly to α-Fe_2O_3 on heating above 700 K. There is also a possibility that Fe_3O_4 (magnetite) nanoparticles may be present. Its most prominent line is (311) which is coincident with that due to the γ-Fe_2O_3 particles. The next most prominent line (220) belonging to magnetite nanocrystals, however, cannot be traced in the XRD spectrum.

TEM images of powder specimens of Fe10 samples calcined at 700 and 1000 °C, respectively (figures 2(a) and 3(a)), show elongated NPs (due to γ-Fe_2O_3) as well as nearly spherical NPs (due to α-Fe_2O_3) [43]. Spherical α-Fe_2O_3 NPs are more in abundance in 1000 °C calcined Fe_2O_3 nanocrystals. High resolution TEM (HRTEM) images shown in figures 2(b) and 3(b) reveal the highly crystalline nature of α-Fe_2O_3 and γ-Fe_2O_3 NPs. The corresponding fast-Fourier transforms of TEM images are shown in figures 2(c) and 3(c). The sizes of Fe_2O_3 NPs measured from TEM images are in fair agreement with those obtained from XRD data (table 1).

3.2. EPR spectra

RT EPR spectra of Fe10 samples (figure 4(a)) have shown the presence of a broad weak signal at $g \sim 4.3$ besides a narrow signal at $g \sim 2.0$. The signal at $g \sim 4.3$ may be assigned to isolated Fe^{3+} ions situated at a highly distorted low-symmetry site [44]. Its intensity becomes progressively less for samples calcined at higher temperatures. This may be due to the migration of these Fe^{3+} ions to some sites to form/add to Fe_2O_3 clusters/NPs at higher temperatures. The sharp EPR signal at $g \sim 2.0$ may be assigned to superparamagnetic single-domain Fe_2O_3 nanocrystals grown in the diamagnetic silica glass

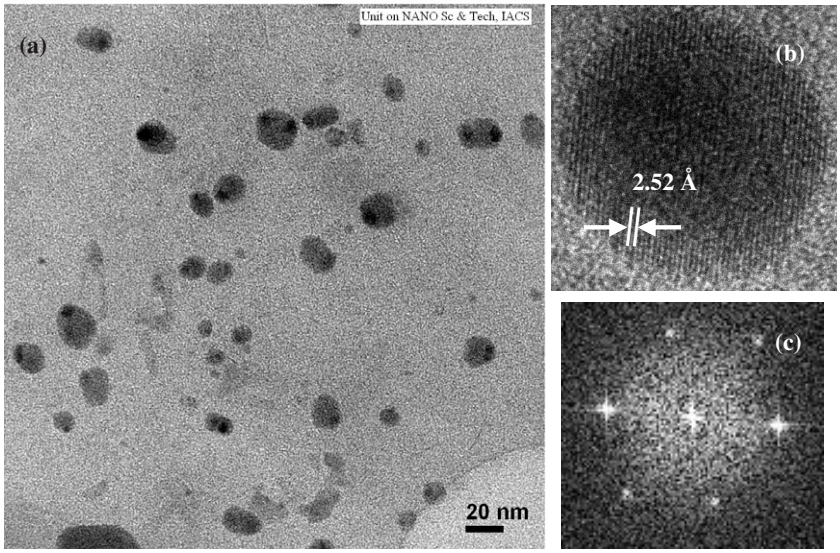

Figure 2. (a) High-magnification TEM images of Fe_2O_3 nanoparticles calcined at 700 °C. (b) The HRTEM image and (c) the corresponding fast-Fourier transform of the TEM images.

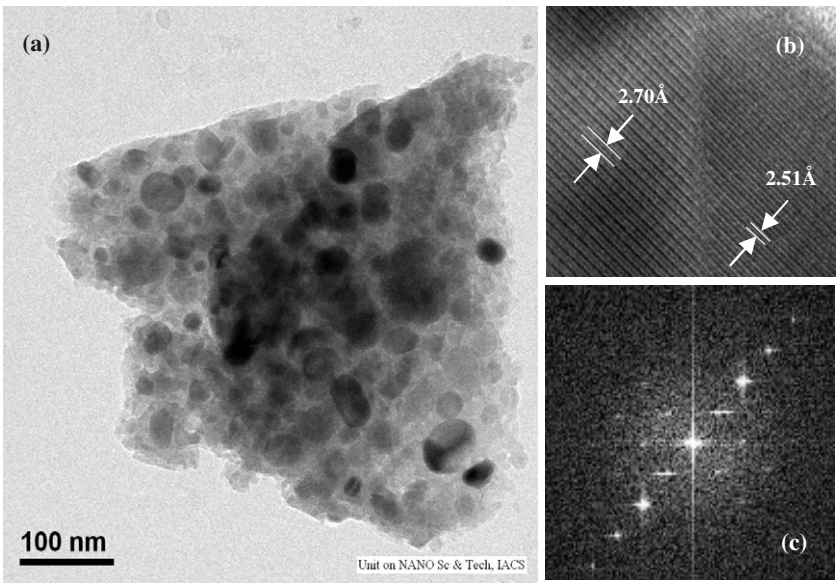

Figure 3. (a) High-magnification TEM images of Fe_2O_3 nanoparticles calcined at 1000 °C. (b) The HRTEM image and (c) the corresponding fast-Fourier transform of the TEM images.

Table 1. Particle size from XRD, TEM and EPR derivative linewidths (ΔH_{pp}) of Fe10 samples calcined at various temperatures at RT and LNT.

Calcination temperature (°C)	Particle size from powder XRD (nm)		Particle size from powder TEM (nm)		ΔH_{pp} (Oe)	
	α-Fe_2O_3	γ-Fe_2O_3	α-Fe_2O_3	γ-Fe_2O_3	RT	LNT
700	11	10	14	12	260	740
800	17	15	—	—	280	860
900	22	20	—	—	210	1000
1000	40	35	45	37	190	1120

matrix calcined at various temperatures [27]. It is significant to note that an increase in the calcination temperature from 800 to 1000 °C results in a considerable decrease in linewidth from 280 to 190 Oe. In this context it is relevant to mention here the important findings of Raman spectroscopic and other studies (including measurements of pore size, density and

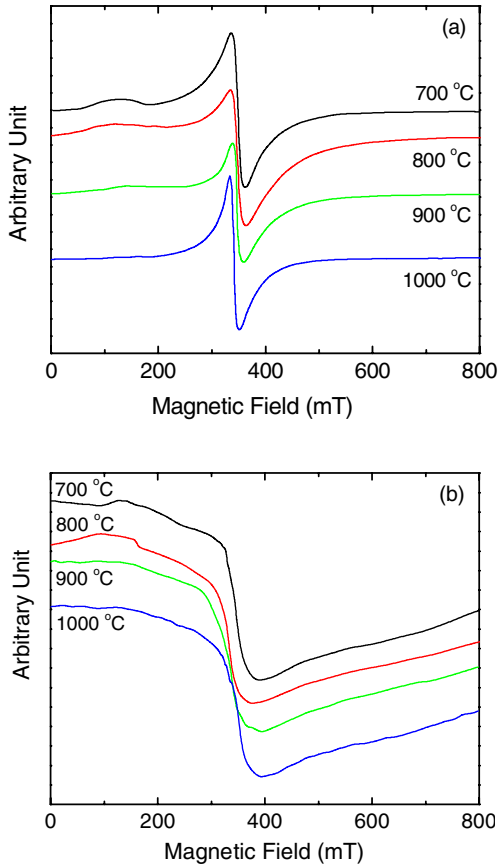

Figure 4. EPR spectra of Fe10 samples recorded at (a) room temperature (RT) and (b) liquid nitrogen temperature (LNT).

specific surface area) [42] on the densification of undoped SiO_2 gel as a function of heat treatment between 120 and 900 °C, i.e. the average pore size increases with increasing calcination temperature and a sudden increase in pore size occurs in the temperature region 700–800 °C (the average pore size increases from 1.0 nm at 700 °C to 2.3 nm at 800 °C), while the specific surface area decreases from 550 to 160 $m^2\ g^{-1}$ and the pore volume/g decreases from 0.19 to 0.12 $cm^3\ g^{-1}$. It is likely that single Fe(III) ions occupy the smallest pores and are responsible for the broad weak EPR signal observed at $g \sim 4.3$. Small pores collapse at higher temperatures, because of their higher surface energy. The surface energy is also influenced by the hydroxyl coverage of the gel and is higher for a silioxane surface than for a hydroxyl surface. With increasing temperature ≡Si–OH groups condense to ≡Si–O–Si≡ bonds, thus increasing the surface energy and enhancing pore collapse. Thus at 800 °C a significant number of small pores collapse and individual Fe ions, set free after the collapse of the small pores, agglomerate to form NPs. The rest of the pores join to form larger pores. At a still higher temperature, namely 900 °C, collapse of larger pores also takes place, similar to what has been observed in an undoped silica sample indicated by a rapid fall of pore volume/g from 0.12 to 0.026 $cm^3\ g^{-1}$ in going from 800 to 900 °C [42]. A Raman spectral study has also revealed that at 900 °C the surface Si–OH groups have completely disappeared, condensing to ≡Si–O–Si≡ bonds and thereby increasing the surface energy and leading to almost complete annihilation of pores. Thus it is possible that at the highest temperature employed in the present case, i.e. 1000 °C, Fe_2O_3 NPs grow to bigger sizes and become closer to each other due to solidification of the gel as a result of the near annihilation of pores. This results in a considerable increase in the inter-nanoparticle exchange interaction, leading to further narrowing of the signal.

LNT spectra (figure 4(b)) reveal profound changes in the lineshapes and the linewidths of the spectra as compared to those recorded at RT. The derivative linewidths ΔH_{pp} obtained at RT and LNT are shown in table 1. It is clearly seen that at LNT, the spectra of all samples become very much broadened and asymmetric and their centres appear to shift to lower magnetic fields. The broadening and shift to lower magnetic fields of the EPR spectra with the decrease of temperature are typical of superparamagnetic NPs [16, 27, 28]. Traditionally [45], narrow (at RT) and broad (at LNT) EPR signals in magnetic NP systems are attributed to superparamagnetic and FM resonances, respectively. In the case of NPs having axial magnetic anisotropy, the following relation for the resonance field was derived by Koksharov *et al* [28]:

$$H_R = \frac{h\nu}{g\beta} - \alpha(|K|/M)(1 - 2/x) + \Delta N L(x)$$

where, $x = VHI_S/kT$, considering all NPs to have the same intrinsic moment I_S, the same volume V and the same anisotropy constant K. The applied field H must be strong enough to cause the relation $HI_S \gg |K|$ to be true. $L(x)$ is the Langevin function. The anisotropy field (H_A) is expressed as $H_A = |K|/M$ (M is the sample magnetization). The demagnetization field (H_S) depends on the shape of the sample and is expressed as $H_S = -\Delta NM$. ΔN is called the anisotropy form factor and is a function of the sample dimensions. At high temperatures ($x \ll 1$), the anisotropy and demagnetization fields for NP system tend to zero. In this case a narrow EPR signal is observed at $H_R \approx \frac{h\nu}{g\beta}$. This is the so-called superparamagnetic resonance [45]. At low temperature, H_A and H_S tend to have their bulk values and broad signal of the FM resonance should be obtained. This is what is observed in the Fe10 sample calcined at the highest temperature 1000 °C of our experiment. In this case ΔH_{pp} has shown about a six times increase in going from RT to LNT. We could not, however, detect resolved magnetic resonance signals due to α-Fe_2O_3 and γ-Fe_2O_3 nanocrystals which, as per the XRD findings, are present in silica glass in comparable proportions.

3.3. Mössbauer spectroscopy

^{57}Fe Mössbauer spectra of samples calcined at temperatures of 800, 900 and 1000 °C are recorded at RT (figures 5(a)–(c)), while those of the Fe10 sample calcined at 700 °C are recorded at RT as well as at 100 K (figures 6(a) and (b)). Unlike EPR, Mössbauer measurements have revealed resolved spectra due to α- and γ-Fe_2O_3 nanocrystals. Spectra are simulated by peaks with Lorentzian shape, using a least square fitting method with 5% uncertainty in the estimation of Mössbauer

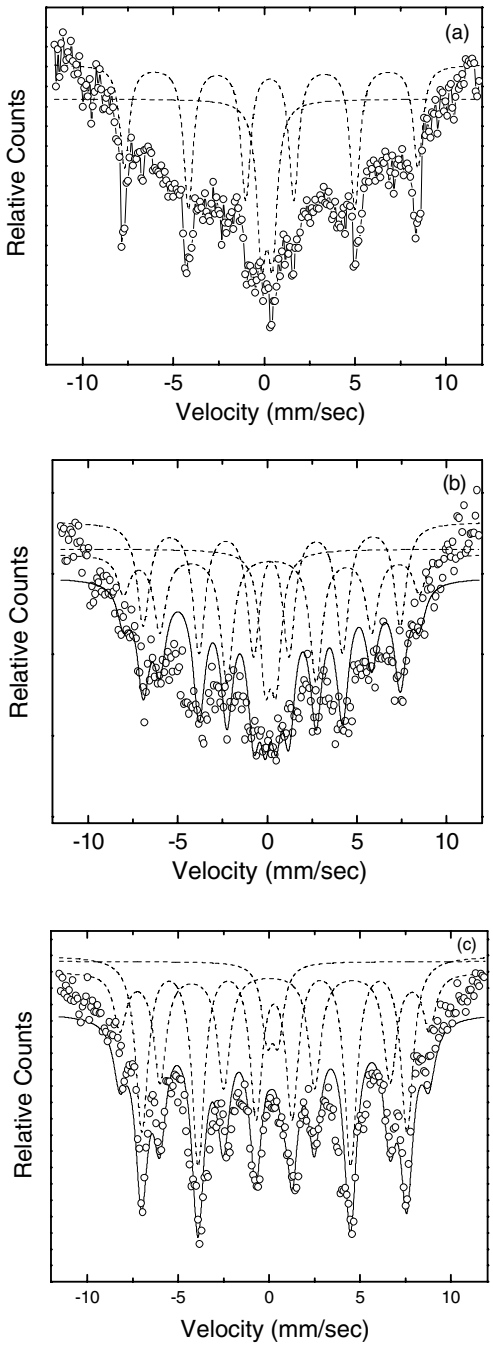

Figure 5. Mössbauer spectra of Fe10 samples calcined at (a) 800 °C, (b) 900 °C and (c) 1000 °C recorded at RT.

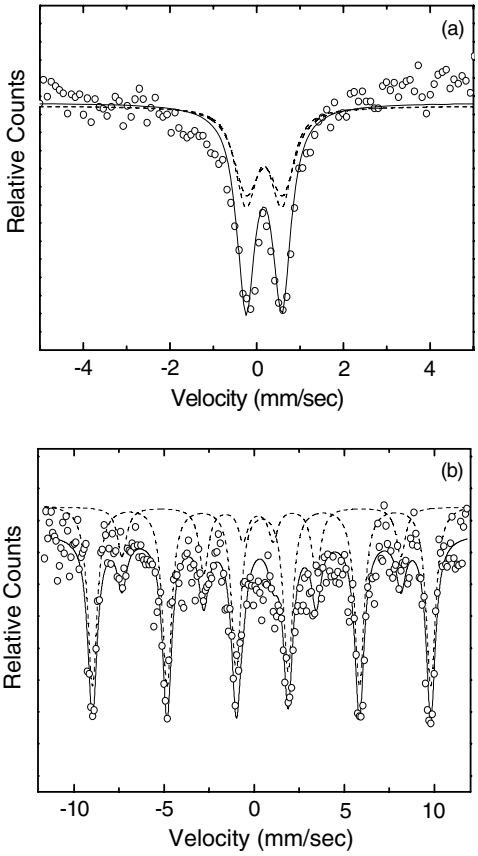

Figure 6. Mössbauer spectra of Fe10 samples calcined at 700 °C recorded at (a) RT and (b) 100 K.

parameters. The fitted Mössbauer parameters, i.e. magnetic hyperfine field (H_{hf}), electric quadrupole splitting (ΔE_{Q}), quadrupole shift (ε), isomer shift (δ) and relative fractions of γ-Fe_2O_3 and α-Fe_2O_3 NPs, are shown in table 2. The values of quadrupole splitting and isomer shift are typical of Fe^{3+} ions of Fe_2O_3 NPs [46]. The transformation, which occurs as a result of calcination at various temperatures, is the evolution of doublets into magnetically split hyperfine (hf) sextets through a series of complicated spectra composed of doublets and sextets. The doublet represents the fraction of small sized NPs in which long-range magnetic ordering is absent. The Fe10 sample calcined at 700 °C shows two doublet structures at RT (figure 6(a)) and two hf sextet spectra at 100 K (figure 6(b)) having a slight asymmetry in the linewidth as well as in the intensity. Two symmetrical quadrupolar doublets obtained at RT are thus transformed into two hf sextets at 100 K, signifying the transformation of superparamagnetic states of α- and γ-Fe_2O_3 NPs into ferromagnetically (FM) ordered states at low temperature. The RT spectrum of the Fe10 sample calcined at 800 °C reveals, instead of two doublets as found in the case of 700 °C calcined sample, one doublet and one hf sextet superimposed on one another. This implies that both superparamagnetic and ferromagnetically ordered components are present in the sample at RT. Analysis of the sextet indicates a distribution of magnetic H_{hf}s due to the particle size distribution. Simulation of the RT spectrum of the Fe10 sample calcined at 900 °C reveals additionally the existence of a sextet over and above a doublet and a sextet structure. This signifies the creation of another magnetically ordered component in the sample on calcination at 900 °C. The intensity of the sextet is more in Fe10 samples calcined at higher temperatures, indicating that larger sized Fe_2O_3 NPs are magnetically ordered even at room temperature. The fitted Mössbauer parameters are consistent with those reported for γ-Fe_2O_3 and α-Fe_2O_3 bulk crystals [46, 47]. From analysis of the spectrum of Fe10 sample calcined at 1000 °C, the presence of two hf sextets corresponding to two kinds of magnetically ordered states of Fe_2O_3 NPs has been confirmed. A weak superparamagnetic doublet has also been identified.

Table 2. Mössbauer parameters—quadrupole splitting (ΔE_Q), isomer shift (δ), magnetic hyperfine field (H_{hf}), quadrupole shift (ε) and relative fraction—for α-Fe_2O_3 and γ-Fe_2O_3 nanocrystals as obtained from fitting of the Mössbauer spectra of Fe10 samples calcined at various temperatures up to 1000 °C recorded at room temperature.

Fe site	Calcination temperature (°C)	ΔE_Q (mm s^{-1})	ε (mm s^{-1})	H_{hf} (T)	δ (mm s^{-1})	Relative fraction (%)
α-Fe_2O_3	700	0.840	—	—	0.18	54
	700[a]	—	−0.084	58.5	0.50	54
	800	—	−0.080	52.9	0.36	60
	900	—	−0.075	51.4	0.25	60
	1000	—	−0.070	50.7	0.32	70
γ-Fe_2O_3	700	0.830	—	—	0.16	46
	700[a]	—	0.04	48.2	0.32	46
	800	0.64	—	—	0.15	40
	900	0.63	—	—	0.19	15
		—	−0.02	45.3	0.20	25
	1000	0.60	—	—	0.20	5
		—	0.00	44.7	0.29	25

[a] Spectra recorded at 100 K.

From table 2 it is seen that both γ-Fe_2O_3 and α-Fe_2O_3 NPs are present in nearly equal proportion (23:27) in the 700 °C calcined sample. But in Fe10 samples calcined at higher temperatures gradual conversion of γ-Fe_2O_3 NPs to α-Fe_2O_3 NPs is observed. In Fe10 samples calcined at 1000 °C, the relative population of γ-Fe_2O_3 and α-Fe_2O_3 NPs is 25:70. Further, it is significant to note that, at RT, while α-Fe_2O_3 NPs contained in the 800, 900 and 1000 °C calcined Fe10 samples are magnetically ordered, γ-Fe_2O_3 NPs are found to be in the magnetically ordered state only in the 900 and 1000 °C calcined Fe10 samples.

In case of non-interacting magnetic NPs, the hf sextet observed at low temperature (100 K) becomes a doublet at room temperature (293 K) because of fast superparamagnetic relaxation [23]. This is true for α-Fe_2O_3 and γ-Fe_2O_3 NPs present in the 700 °C calcined sample. RT Mössbauer spectra of samples calcined at higher temperatures (800, 900 and 1000 °C) reveal hf sextets due to α-Fe_2O_3 NPs. It is also noticed that with increasing calcination temperature the hf lines become asymmetrically broadened and the average hyperfine field diminishes in a way typical for interacting magnetic NPs [18, 22, 25] (table 2). This is expected, because in samples calcined at higher temperatures (particularly at 1000 °C) NPs are larger and more closely spaced because of collapse of pores and become exchanged coupled. This means that, for near agglomerated NPs, superparamagnetic relaxation is suppressed and the doublet is transformed into a hf sextet conforming to an ordered state in which the exchange interaction energy is predominant compared to the anisotropy energy. The line broadening of the sextets in these spectra may be accounted for on the basis of varying exchange interactions present in the samples. The sublattice magnetization direction in the assembly of AFM α-Fe_2O_3 NPs may be influenced by interparticle exchange interaction. This may lead to a rotation of the sublattice magnetization from the direction defined by the magnetic anisotropy [48]. The quadrupole shift (ε) is given by the relation $\varepsilon = \frac{1}{2}(3\cos^2\theta - 1)\Delta E_Q$, where ΔE_Q is the quadrupole splitting and θ is the angle between the sublattice magnetization direction and the [001] axis. The computed values of ε and of θ for α-Fe_2O_3 NPs calcined at 800, 900 and 1000 °C are shown in table 2. These are −0.080, −0.075 and −0.070 and 75°, 73° and 71°, respectively. Thus, for interacting α-Fe_2O_3 NPs, deviation of the ε values from −0.100 mm s^{-1} suggests an out-of-plane rotation of the sublattice magnetization.

The hf parameters obtained for γ-Fe_2O_3 NPs are also listed in table 2. It is noted that the intensity of the sextet with respect to that of the doublet is more in the samples calcined at higher temperatures, indicating that a greater number of γ-Fe_2O_3 NPs become magnetically ordered at higher calcination temperatures. The hf magnetic fields are found to have lower values in γ-Fe_2O_3 NPs (48.2–44.7 T) compared to these in the bulk crystal. This has been ascribed to the effect of collective magnetic interaction [49].

3.4. Magnetization

3.4.1. FC and ZFC mass magnetization. FC and ZFC magnetizations of Fe10 samples calcined at 700, 800 and 900 °C are measured in the presence of 200 Oe dc magnetic field as a function of temperature in the temperature range 5–300 K. ZFC and FC curves (figure 7) show divergent behaviours at low temperatures. The FC curve of the Fe10 sample calcined at 700 °C shows a monotonic increase with decreasing temperature down to the lowest temperature of 5 K (the rate of increase is more at low temperatures). The ZFC curve at first slowly increases with lowering of the temperature following the same path as that of the FC curve, then starts deviating from the latter curve at ∼200 K, subsequently exhibits a broad peak at ∼65 K (identified as the blocking temperature T_{B1} pertaining to α-Fe_2O_3 NPs [16]) and another at 16 K (assigned as the blocking temperature T_{B2} due to γ-Fe_2O_3 NPs [9]) and then decreases down to 5 K. Such behaviour is akin to superparamagnetism [50, 51]. Thermal behaviours of ZFC and FC curves of Fe10 samples calcined at 800 and 900 °C are also quite similar. Two maxima in the ZFC mass magnetization curves are detected at increasingly higher temperatures (table 3a). The higher T_B values indicate

Table 3a. Temperatures corresponding to the maxima in the ZFC curves (T_{B1}, T_{B2}), remanent magnetization (M_r), coercive field (H_c), ratio of remanent magnetization and magnetization measured at 6 T (M_r/M_{6T}) for the Fe10 samples calcined at 700, 800 and 900 °C, evaluated from static mass magnetization and hysteresis measurements at different temperatures.

Fe10 sample calcined at	T_B (K)		M_r (A m^2 kg^{-1})		H_c (T)		M_r/M_{6T}	
	T_{B1} (α-Fe_2O_3)	T_{B2} (γ-Fe_2O_3)	300 K	5 K	300 K	5 K	300 K	5 K
700 °C	65	16	0	0.009	0	0.125	0	0.19
800 °C	106	21	0.002	0.012	0.037	0.135	0.07	0.22
900 °C	110	25	0.003	0.021	0.062	0.237	0.09	0.29

Table 3b. Blocking temperatures (T_{B1} and T_{B2}) corresponding to the maxima in the ZFC curves for α- and γ-Fe_2O_3 nanoparticles, remanent magnetizations (M_r), coercive fields (H_c) and spin–flop fields (H_{sf}) at different temperatures for Fe10 samples calcined at 1000 °C, evaluated from static mass magnetization and hysteresis measurements under ZFC and FC conditions. (Values within parentheses are under FC conditions.)

	ZFC magnetization						
	α-Fe_2O_3	γ-Fe_2O_3	Hysteresis			Spin–flop field (H_{sf})	
Field (T)	T_{B1} (K)	T_{B2} (K)	T (K)	H_c (T)	M_r (A m^2 kg^{-1})	ZFC hysteresis (T)	
0.2	155	—	300	1.875 (1.869)	0.065 (0.067)	2.084 (—)	
1.0	152	—	140	0.616 (0.554)	0.077 (0.076)	0.536 (0.780)	
3.0	143	30	5	0.807 (0.827)	0.063 (0.067)	1.405 (1.328)	

that the NPs have larger average energy barriers. Since the energy barrier is proportional to the volume, the larger T_B values signify that larger sized NPs are generated in the samples treated at higher calcination temperatures. This is consistent with XRD and TEM results. But there is no trace of a Morin transition in these samples in the temperature range 5–300 K (figures 7(a)–(c)). The nature of ZFC and FC versus temperature curves of Fe10 samples calcined at 1000 °C, however, is quite different (figure 8(a)). FC and ZFC curves with 200 Oe applied field are at first coincident (starting from RT) and show increase with decreasing temperature down to 160 K followed by a decrement down to 120 K. A broad peak is observed at ∼155 K which may be assigned as the blocking temperature T_{B1}, revealing the superparamagnetic character of α-Fe_2O_3 NPs of sizes in the vicinity of 40 nm (see table 1). The two curves then undergo a steep fall starting from ∼120 K down to ∼90 K, displaying the characteristic Morin transition as in the case of bulk α-Fe_2O_3 crystals but with much depressed transition temperature T_M about 100 K. (For bulk crystal T_M is ∼260 K.) This is more elegantly demonstrated from the $d\sigma/dT$ versus T curve (inset of figure 8(a)). A sharp peak is observed at ∼103 K which is identified as T_M. Below the Morin transition the ZFC and FC curves follow different paths. While the ZFC curve shows a slow monotonic decrement down to 5 K, the FC curve has a slow continuous rise from 50 to 5 K. However, in presence of higher magnetic fields of 1 and 3 T the Morin transition is weakened to the extent of being wiped out (figures 8(b) and (c)). Thus it appears that an applied dc magnetic field of adequate magnitude could effect suppression of the Morin transition. A small maximum is observed at ∼30 K in the ZFC magnetization curve obtained under a 3 T dc field which may be labelled as the blocking temperature T_{B2} belonging to γ-Fe_2O_3 NPs (table 3b).

As regards the evidence for the presence of magnetite nanocrystals it is relevant to examine here the detailed magnetic studies of Goya *et al* [52] on Fe_3O_4 NPs with average particle sizes ranging from 5 to 150 nm. Bulk-like properties such as the Verwey transition ($T_v = 98$ K) have been observed in 150 nm particles. For decreasing particle size, the Verwey temperature T_v shifts towards lower temperature. The sample containing 50 nm particles shows a kink at ∼20 K in the ZFC curve probably related to the Verwey transition. However, the Verwey transition remains unobserved for particles having sizes of less than 50 nm. Since the particles in our samples have sizes of less than 50 nm, the presence of Fe_3O_4 nanoparticles could not be ascertained from ZFC curves obtained by us in terms of the Verwey transition.

3.4.2. Magnetic hysteresis. DC magnetization versus magnetic field curves for the Fe10 samples calcined at 700, 800 and 900 °C are plotted at two temperatures 300 and 5 K in the dc magnetic field range ±6 T (figures 9(a)–(c)). The values of coercive field (H_c) and remanent magnetization (M_r) evaluated from hysteresis loops are shown in table 3a. It is significant to note that Fe_2O_3 NPs of Fe10 sample calcined at 700 °C do not display any hysteresis loop at 300 K. This may be due to the fact that the 700 °C calcined Fe10 sample is in the superparamagnetic state at 300 K. However, at 5 K, a hysteresis loop is obtained and the coercive field is found to have a non-zero value ($H_c = 0.125$ T). This means that at 5 K the NPs are in a magnetically ordered state. On the other hand, Fe10 samples calcined at higher temperatures, i.e. 800 and 900 °C, display magnetic hysteresis loops even at 300 K, indicating that Fe_2O_3 NPs embedded in silica matrices are magnetically ordered. These results are in agreement with our RT Mössbauer findings. However, it is to be noted that hysteresis loops due to α- and γ-Fe_2O_3 NPs could not be distinguished. At 300 K, as well as at 5 K, the coercive fields associated with Fe_2O_3 NPs are found to be greater for

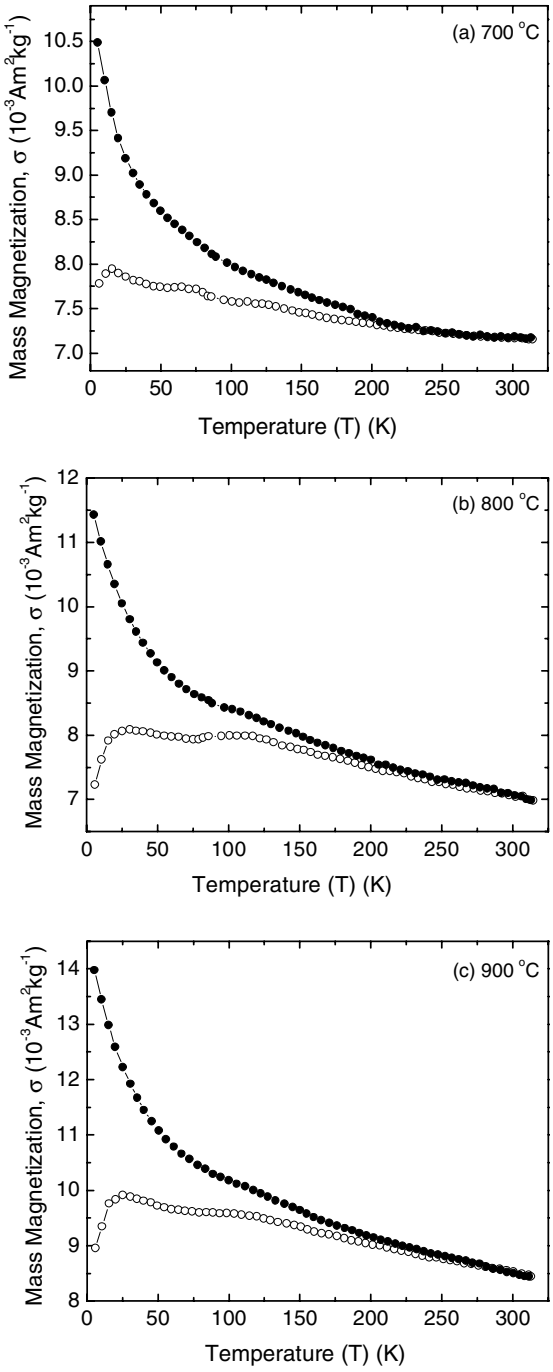

Figure 7. ZFC (○) and FC (●) mass magnetization versus temperature curves for Fe10 samples calcined at (a) 700 °C, (b) 800 °C and (c) 900 °C (applied DC magnetic field 200 Oe).

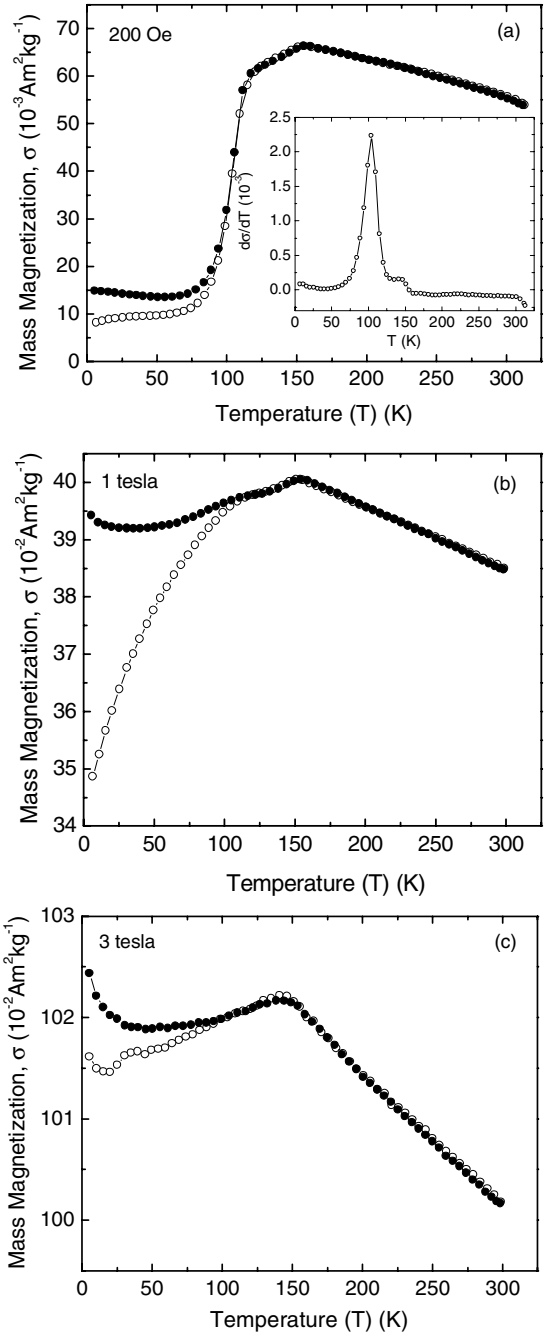

Figure 8. ZFC (○) and FC (●) mass magnetization versus temperature curves for Fe10 samples calcined at 1000 °C with applied DC magnetic field (a) 200 Oe, (b) 1 T and (c) 3 T. (Inset: $d\sigma/dT$ versus T.)

Fe10 samples calcined at higher temperatures. The ratio of remanent magnetization and magnetization measured at 6 T (M_r/M_{6T}) also shows a similar trend. Magnetizations in applied magnetic fields up to 6 T on Fe10 samples calcined at 700, 800 and 900 °C at 300 and 5 K are shown in figure 10. The magnetization curves first show a linear increase with the magnetic field, then a downward curvature, followed by a linear increase at high fields. This suggests that there are two contributions to the magnetization M [53], which is expressed as $M = M_0[\coth(x) - 1/x] + \chi H$, where M_0 is the saturation magnetization, $x = \mu_p H/kT$, μ_p being the average magnetic moment of α-Fe_2O_3 arising from uncompensated surface spins, and χ is the magnetic susceptibility.

ZFC and FC magnetizations as a functions of magnetic field (up to 6 T) of the Fe10 sample calcined at 1000 °C are recorded at three different temperatures, namely 300, 140 and 5 K (figure 11). The data are collected from the hysteresis loops obtained at different temperatures (figure 12) after cooling the sample from room temperature down to 5 K

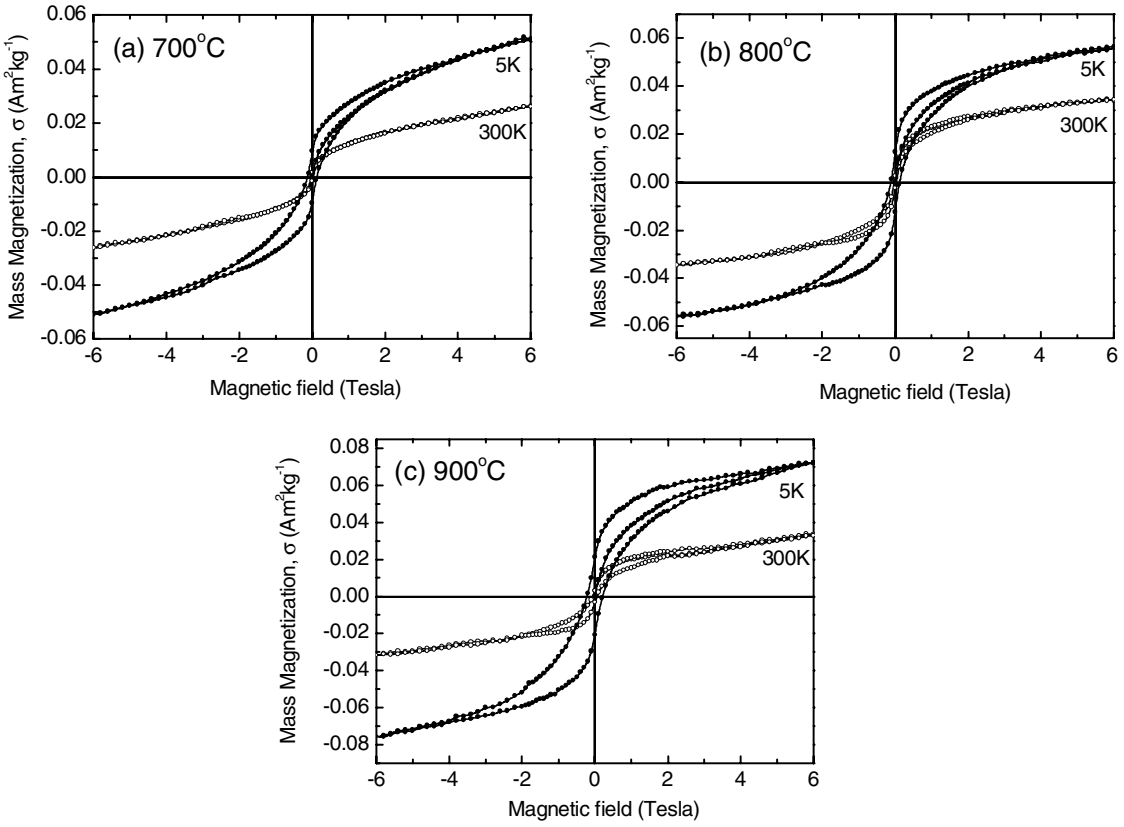

Figure 9. Hysteresis loops of Fe10 samples calcined at (a) 700 °C, (b) 800 °C and (c) 900 °C recorded at 300 and 5 K.

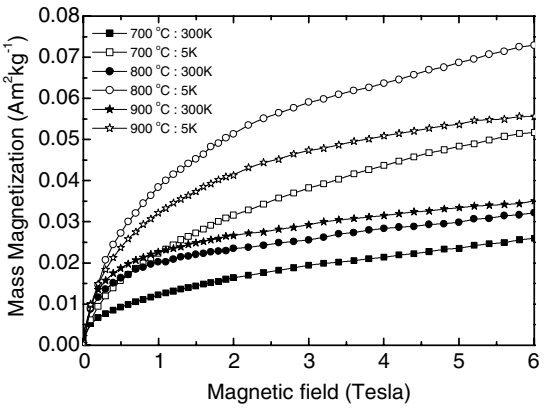

Figure 10. Mass magnetization versus H curves of Fe10 samples calcined at 700, 800 and 900 °C recorded at 300 and 5 K.

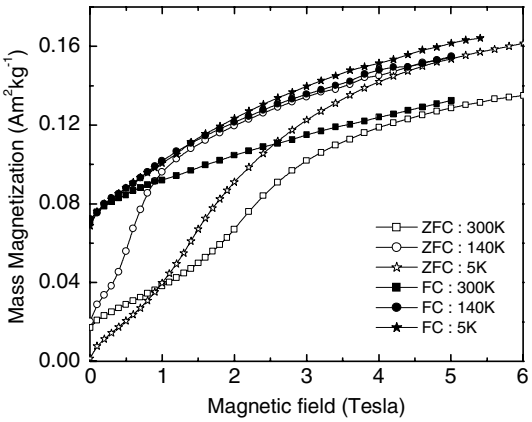

Figure 11. ZFC and FC mass magnetization versus H curves of Fe10 samples calcined at 1000 °C and recorded at 300, 140 and 5 K.

without a magnetic field (ZFC hysteresis) and also cooling the sample in an applied field of 5 T (FC hysteresis) down to 5 K, then switching off the field and measuring the field-dependent magnetization at increasing temperatures (5, 140 and 300 K). A change of curvature, signalling the spin–flop transition, is observed to occur within the magnetic field range 0–5 T. The spin–flop transition field (H_{sf}) may be conveniently taken as the field corresponding to the maximum occurring in $d\sigma/dH$ versus H curve (figure 13). H_{sf} values obtained at different temperatures for ZFC and FC conditions are shown in table 3b. It is quite exceptional to discover, from the ZFC hysteresis curve, the presence of a spin–flop transition at moderately high field (2.084 T) even at 300 K which is much above 103 K, the Morin temperature determined for α-Fe_2O_3 NPs (~40 nm diameter) obtained from Fe10 samples calcined at 1000 °C. The above measurements have been repeated several times with fresh samples and the same result has been obtained in each case, confirming that the observation is not erroneous. It is possible that at the highest calcined temperature, i.e. 1000 °C, due to solidification of

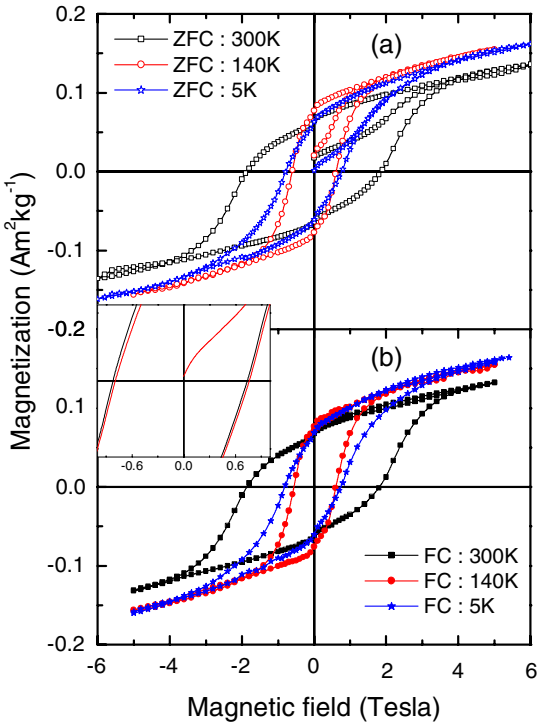

Figure 12. ZFC (a) and FC (b) hysteresis loops of Fe10 samples calcined at 1000 °C and recorded at 300, 140 and 5 K. In the inset, the region close to the displacement of the loop shift is highlighted.

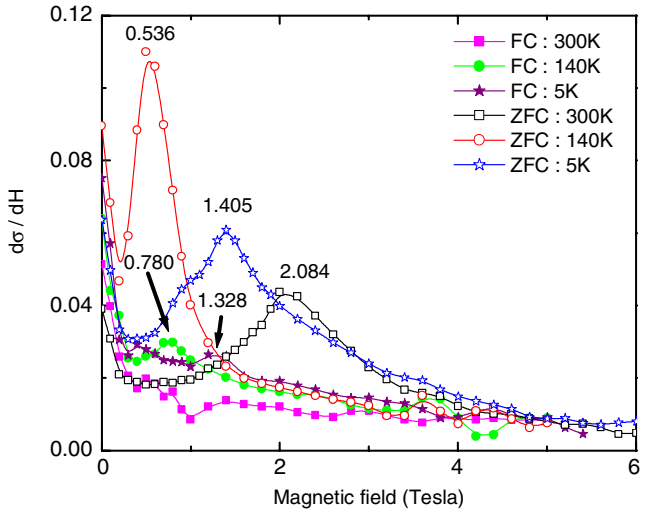

Figure 13. Field derivative of magnetization of Fe10 samples calcined at 1000 °C and recorded at 300, 140 and 5 K.

the gel–glass as a result of annihilation of nearly all pores, α-Fe_2O_3 NPs become much closer to one another, leading to significant interparticle exchange interaction which may be responsible for the existence of the spin–flop transition at ambient temperature which is much above the Morin temperature of bulk α-Fe_2O_3 (260 K). Further, interparticle exchange interaction with γ-Fe_2O_3 NPs (present in significant numbers) may play some role in this regard. It is noted that the spin–flop transition field H_{sf} at 140 K is smaller than that at 300 K but it has a higher value at 5 K. It is interesting to note that the thermal behaviours of coercivity (H_c) and H_{sf} are quite similar (table 3b). It may be relevant to mention here the theoretical works of Schulthes and Butler [54] on magnetic properties of FM/AFM bilayers based on a microscopic Heisenberg model. It is shown that the spin–flop coupling gives rise to a uniaxial anisotropy which in turn causes large coercivities and thus H_{sf} and H_c might be closely related. This is in conformity with our present experimental observations.

The hysteresis loop obtained (figure 12(b)) after field cooling under 5 T is more irreversible at high field. For the Fe10 sample calcined at 1000 °C at 5 K, the observed displacement of the loop (∼400 Oe) reveals the presence of an exchange field H_e (in exchange anisotropy [55, 56] terminology), which arises due to the exchange coupling between the different core and surface magnetic structures of antiferromagnetically (uncompensated) ordered and frozen disordered, respectively. This is observed in other antiferromagnet NP systems [57]. H_e decreases rapidly with increasing temperature and is negligibly small at $T = 140$ K.

4. Conclusions

The principal findings of the present investigation of sol–gel derived Fe_2O_3 NPs in silica matrix are summarized below:

(i) The narrow superparamagnetic resonance line observed in Fe10:SiO_2 glass at room temperature is transformed to a broad highly asymmetric ferromagnetic resonance signal at low temperature (77 K).

(ii) (a) RT Mössbauer measurements of the sample calcined at 700 °C show two doublets due to γ-Fe_2O_3 and α-Fe_2O_3 NPs demonstrating their superparamagnetic character, whereas in the case of samples calcined at 1000 °C two hyperfine sextets have been observed indicating that both α- and γ-forms of Fe_2O_3 NPs are in a magnetically ordered state at room temperature.

(b) At higher calcination temperatures the hyperfine lines become asymmetrically broadened and the average hyperfine field diminishes in a way typical for interacting magnetic NPs.

(iii) (a) Magnetic measurements, including magnetic hysteresis, show unusual ferromagnetic-like behaviour with substantial magnetization and coercivity values at low temperature (5 K) for Fe10 samples calcined at higher temperatures although α-Fe_2O_3 NPs, in comparison to γ-Fe_2O_3 NPs, are more abundant in Fe_2O_3 samples calcined at higher temperatures. The observed ferromagnetism of α-Fe_2O_3 NPs (bulk α-Fe_2O_3 is antiferromagnetic) at low temperature may be ascribed to the uncompensated surface spins present on the antiferromagnetic core of the α-Fe_2O_3 NPs.

(b) High coercive fields, high irreversibility fields and shifted hysteresis loops are some of the features associated with Fe10 samples calcined at 1000 °C which possibly arise from the combined effects of the uniaxial anisotropy, surface anisotropy and exchange anisotropy.

(c) Both Morin and spin–flop like transitions are only observed in α-Fe_2O_3 NPs present in Fe10 samples calcined at 1000 °C. Due to the finite size effect, the values of the Morin temperature and spin–flop fields are significantly below those observed in bulk α-Fe_2O_3 crystals. Observation of the spin–flop like transition at temperatures above the Morin temperature is a surprising result. The presence of FM/AFM interface exchange in α-Fe_2O_3 nanoparticles, along with inter-nanoparticle exchange including those with γ-Fe_2O_3 nanoparticles (which are present in significant numbers) may be responsible for the observation of the spin–flop like transition in α-Fe_2O_3 nanoparticles even at 300 K.

(iv) The presence of Fe_3O_4 nanoparticles in our Fe10 samples cannot be definitely ascertained from XRD or Mössbauer spectra. The characteristic Verway transition due to Fe_3O_4 nanoparticles cannot be located in the ZFC/FC curves obtained in the 5–300 K temperature range, presumably because of their small sizes (less than 50 nm). Under the circumstances, the presence of a small percentage of Fe_3O_4 nanoparticles in our samples cannot be ignored.

References

[1] Dormann J L, Tronc E and Fiorani D 1997 *Advances in Chemical Physics* vol 98 (New York: Wiley) pp 283–494
[2] Dormann J L and Fiorani D (ed) 1992 *Magnetic Properties of Fine Particles* (Amsterdam: North-Holland)
[3] Zysler R D, Vasquez Mansilla M and Fiorani D 2004 *Eur. Phys. J.* B **41** 171
[4] Xu X N, Wolfus Y, Shaulov A, Yeshurun Y, Felner I, Norwik I, Koltypin Yu and Gedanken A 2002 *J. Appl. Phys.* **91** 4611
[5] Goya G F, Veith M, Rapalavicuite R, Shen H and Mathur S 2005 *Appl. Phys.* A **80** 1523
[6] Uhm Y R, Kim W W, Kim S J, Kim C S and Rhee C K 2003 *J. Appl. Phys.* **93** 7196
[7] Jiao F, Harrison A, Jumas J-C, Chadwick A V, Kockelmann W and Bruce P G 2006 *J. Am. Chem. Soc.* **128** 5468
[8] Vasquez-Mansilla M, Zysler R D, Arciprete C, Dimitrijewits M I, Saragovi C and Greneche J M 1999 *J. Magn. Magn. Mater.* **204** 29
[9] Cannas C, Concas G, Gatteschi D, Falqui A, Musinu A, Piccaluga G, Sangregorio C and Spano G 2001 *Phys. Chem. Chem. Phys.* **3** 832
[10] Dormann J L, Fiorani D, Cherkaoui R, Spinu L, Lucar F, D'Orazio F, Nogub M, Tronc E, Jolivet J P and Garcia A 1999 *Nanostruct. Mater.* **12** 757
[11] Parker F T, Foster M W, Margulies D T and Berkowitz A E 1993 *Phys. Rev.* B **47** 7885
[12] Zysler R D, Fiorani D, Testa A M, Suber L, Agostinelli E and Godinho M 2003 *Phys. Rev.* B **68** 212408
[13] Fiorani D, Testa A M, Suber L, Angiolini M, Montone A and Polichetti M 1999 *Nanostruct. Mater.* **12** 939
[14] Carbone C, Benedetto F Di, Marescotti P, Sangregorio C, Sorace L, Lima N, Romanelli M, Lucchetti G and Cipriani C 2005 *Miner. Petrol.* **85** 19
[15] Martínez B, Obradors X, Balcells Ll, Rouanet A and Monty C 1998 *Phys. Rev. Lett.* **80** 181
[16] Dimitrov D V, Hadjipanayis G C, Papaefthymiou V and Simopoulos A 1998 *J. Magn. Magn. Mater.* **188** 8
[17] Predoi D, Kuncser V, Filoti G and Schinteie G 2003 *J. Optoelectron. Adv. Mater.* **5** 211
[18] Mørup S, Bødker F, Hendriksen P V and Linderoth S 1995 *Phys. Rev.* B **52** 287
[19] Mørup S and Tronc E 1994 *Phys. Rev. Lett.* **72** 3278
[20] Bødker F and Mørup S 2000 *Europhys. Lett.* **52** 217
[21] Pankhurst Q A, Johnson C E and Thomas M F 1986 *J. Phys. C: Solid State Phys.* **19** 7081
[22] Frandsen C and Mørup S 2003 *J. Magn. Magn. Mater.* **266** 36
[23] Xu M, Bahl C R H, Frandsen C and Mørup S 2004 *J. Colloid Interface Sci.* **279** 132
[24] Kündig W, Bömmel H, Constabaris G and Lindquist R H 1966 *Phys. Rev.* **142** 327
[25] Hansen M F, Koch C B and Mørup S 2000 *Phys. Rev.* **62** 1124
[26] Hseih C T, Huang W L and Lue J T 2002 *J. Phys. Chem. Solids* **63** 733
[27] Berger R, Bissey J-C, Kliava J, Daubric H and Estournès C 2001 *J. Magn. Magn. Mater.* **234** 535
[28] Koksharov Yu A, Gubin S P, Kosobudsky I D, Beltran M, Khodorkoversusky Y and Tishin A M 2000 *J. Appl. Phys.* **88** 1587
[29] Koksharov Yu A, Gubin S P, Kosobudsky I D, Yurkov G Yu, Pankratov D A, Ponomarenko L A, Mikheev M G, Beltran M, Khodorkoversusky Y and Tishin A M 2000 *Phys. Rev.* B **63** 012407
[30] Klausen S N, Lefmann K, Lindgård P-A, Theil Kuhn L and Bahl C R H 2004 *Phys. Rev.* B **70** 214411
[31] Morin F J 1950 *Phys. Rev.* **78** 819
[32] Shull C G, Strauser W A and Wollan E O 1951 *Phys. Rev.* **83** 333
[33] Guilland C 1951 *J. Phys. Rad.* **12** 489
[34] Besser P J and Morrish A H 1964 *Phys. Lett.* **13** 289
[35] Artman J O, Murphy J C and Foner S 1965 *Phys. Rev.* **138** A912
[36] Kaczer J and Shalnikova T 1964 *Proc. Int. Conf. on Magnetism (Nottingham)* (London: Physical Society) p 589
[37] Dormann J L, Cui J R and Sella C 1985 *J. Appl. Phys.* **57** 4283
[38] Morrish A H 1994 *Canted Antiferromagnetism: Hematite* (Singapore: World Scientific)
[39] Amin N and Arajs S 1987 *Phys. Rev.* B **35** 4810
[40] Dang M Z, Rancourt D G, Dutrizac J E, Lamarche G and Provencher R 1998 *Hyperfine Interact.* **177** 271
[41] Sakka S and Kamiya K 1982 *J. Non-Cryst. Solids* **48** 31
[42] Krol D M and van Lierop J G 1984 *J. Non-Cryst. Solids* **63** 131
[43] Ayyub P, Multani M, Barma M, Palkar V R and Vijayaraghavan R 1988 *J. Phys. C: Solid State Phys.* **21** 2229
[44] Berger R, Kliava J, Bissey J C and Baïetto V 1998 *J. Phys.: Condens. Matter* **10** 8559
[45] Sharma V K and Waldner F 1977 *J. Appl. Phys.* **48** 4298
[46] Cornell R M and Schwertmann U 1996 *The Iron Oxides* (Weinheim: VCH)
[47] Keller K and Schmidbauer E 1996 *J. Magn. Magn. Mater.* **162** 85
[48] Frandsen C and Mørup S 2005 *Phys. Rev. Lett.* **94** 027202
[49] Brown W F Jr 1963 *Phys. Rev.* **130** 1677
Mørup S, Topsoe H and Lipika J 1976 *J. Physique Coll.* 35 C6 207
[50] Néel L 1949 *Ann. Geophys.* **5** 99
[51] Néel L 1949 *C. R. Acad. Sci. Paris* **228** 664
[52] Goya G F, Berquó T S, Fonseca F C and Morales M P 2003 *J. Appl. Phys.* **94** 3520
[53] Kilcoyne S H and Cywinski R 1995 *J. Magn. Magn. Mater.* **140** 1466
[54] Schulthes T C and Butler W H 1998 *Phys. Rev. Lett.* **81** 4516
[55] Meiklejohn W H and Bean C P 1956 *Phys. Rev.* **102** 1413
Meiklejohn W H and Bean C P 1957 *Phys. Rev.* **105** 904
[56] Meiklejohn W H 1962 *J. Appl. Phys.* **33** 1328
[57] Makhlouf S A, Parker F T, Spada F E and Berkowitz A E 1987 *J. Appl. Phys.* **81** 5561
Makhlouf S A, Parker F T and Berkowitz A E 1997 *Phys. Rev.* B **55** R14719